International Journal of Materials Science and Applications
2023; 12(6): 91-104
http://www.sciencepublishinggroup.com/j/ijmsa
doi: 10.11648/j.ijmsa.20231206.12
ISSN: 2327-2635 (Print); ISSN: 2327-2643 (Online)

Nanoparticle Enhances Fracture Strength in FSP Aluminium Alloys

Paresh Kumar Mandal

Department of Metallurgical and Materials Engineering, Amal Jyothi College of Engineering, Kanjirappally, India

Email address:
pkm.iitr@gmail.com

To cite this article:
Paresh Kumar Mandal. (2023). Nanoparticle Enhances Fracture Strength in FSP Aluminium Alloys. *International Journal of Materials Science and Applications*, *12*(6), 91-104. https://doi.org/10.11648/j.ijmsa.20231206.12

Received: June 28, 2023; **Accepted**: July 25, 2023; **Published**: December 28, 2023

Abstract: The grain refinement effects and the ageing behaviour of aluminium alloys have been studied on the basis of OM, EPMA, FESEM, SEM, TEM, hardness measurements and mechanical properties. Grain refinement markedly achieved due to effectively consider at variable scandium contents (eg. hypereutectic composition) in cast aluminium alloys. The nanoparticles are fully coherent in matrix and its low lattice misfits (1.5%) caused well strong interaction with defects and dispersive characteristic. These alloys potentially revealed nanosized precipitates namely GP-zones, ή/η and Al_3Sc ($L1_2$) particles. The TEM micrographs revealed homogeneous distribution of nanoparticles after T_6 treatment and measured nanosized Al_3Sc particles (30-50 nm) after FSP. The FSP has potentially refine grains which is known to Zener pinning mechanism due to inhibit grain growth. Notably, FSP had been measured after T_4+FSP+Aged at 140°C for 2h (SFA), and related mechanical properties significantly achieved likely UTS of 329 MPa, ductility of 8.9%, hardness of 147.8HV and K_{IC} of 3.42-32.6 MPa√m in SZ, but fracture strength and ductility decline drastically in high scandium contents (0.87 wt.%) about 178 MPa and 4%, respectively. The aim is to determine the fracture strength for dispersive nanosized particles during FSP and subsequently TEM and SEM fractography analysis.

Keywords: $MgZn_2$(ή), Nanosized Al_3Sc Particles, TEM, SEM, FSP, Fracture Strength

1. Introduction

Addition of variable scandium (Sc) contents (eg. hypereutectic composition) in aluminium alloys (7xxx series), it has been found to quicken the ageing kinetics and readily harden the alloys to formation of nanosized Al_3Sc particles during solidification. These inoculation particles are eliminated hot cracking, precipitation free zone (PFZ), and completely grain boundary (GB) segregation during solidification of cast alloys [1-4]. Thus, scandium is well-known to be an active grain refining agent due to eutectic compound (eg. Al_3Sc at 655°C) serving as a potent nucleant in the melt during solidification. The nanosized Al_3Sc dispersoids benefit from the rapid precipitation characteristic of scandium in aluminium, the slow coarsening related mechanism, and the high-volume fraction as an effect of scandium. The Al_3Sc particle is a stable heterogeneous nature and can profoundly refine aluminium grains when the concentration of scandium in the melt exceeds the critical limit. Notably, the high interfacial energy with incoherent interfaces offer to effective heterogeneous nucleation sites, and then stable η phase easily nucleates on the nanosized Al_3Sc particles [5-9]. Many researchers had been quoted on grain refinement achieve by heterogeneous nucleation the use of inoculants and by alloying elements and also grain size is inversely related to the degree of undercooling due to increasing nucleation rate [Rosenhain 1930], [Cibula 1951-1952], [Murthy 2002]. In addition, FSP resulted in a significant breakup of coarse second-phase particles and primary dendrites, created a homogeneous distribution of fine particles in the alloys, and nearly eliminated all casting porosities, GB segregations and dendritic structures in the matrix. Recently several methods have been developed for minimizing the softening and improving the properties of FSW/FSP, such as optimization of process parameters, using external coolants, or low temperature post ageing treatment etc. During FSP the favorable temperature generated for nanosized (eg. Al_3Sc, ή/η) precipitates to boost the mechanical properties of aluminium alloys are better than the traditional techniques, whereas unwanted microstructures resulting from fusion point and uneven cooling rate during solidification encourage low mechanical properties. By

varying FSP tool design and process parameters are identified such as tool rotation speed, traverse speed, and constant axial force for all the unidirectional passes, and desired microstructure may be created in matrix [10-12]. Since FSP is a recently well-known emerging surface modification technology, while creates three distinct regions such as stirring zone (SZ) as temperature rises up to 400-550°C, the thermomechanically-affected zone (TMAZ) as the temperature generates up to 350-400°C, and the heat-affected zone (HAZ) temperature rise up to above 250°C [13-15]. The FSW/FSP is environmentally clean technology as compared to conventional welding processes while temperatures developed below the melting point ($0.6\text{-}0.7T_m$) of materials may avoids interfacial reactions, porosities, and oxide inclusions could be eliminated. According to the nature of metal flow in the SZ during processing, large clusters of Al_3Sc chunky particles are formed in SZ revealed through optical microscopy (OM), electron probe microanalysis (EPMA), field emission scanning electron microscopy (FESEM), scanning electron microscopy (SEM) with EDX analysis, transmission electron microscopy (TEM), and SEM fractography analysis. The effect of processing parameters precisely was investigated showing changes in microstructure, hardness, tensile and fracture toughness properties have been discussed in this work. It is noteworthy that FSP leads to finer and more homogeneous dispersion of nanoparticles (Al_3Sc, ή/η) in the SZ as well as dynamic recrystallization (DRX) is a main mechanism to form a nanosized structure as well as optimized heat input energy (1.1-1.4 kJ/mm) in the matrix [16-18]. On the other hand, these nanosized particles efficiently could be changed the fracture strength and fracture mechanism on the basis of plain strain fracture toughness (K_{IC}) evaluation of these alloys from intergranular cracks to transgranular failures or mostly mixed mode of failures, decrease the high angle grain boundaries, and also improving stress corrosion cracking resistance with ductility. The goal of this work is to examine the effect of nanoparticles distribution in matrix and FSP on the mechanical properties and fracture strength and microstructural changes of aluminium alloys after SFA condition.

2. Materials and Experimental Procedure

The studied aluminium alloys (7xxx series) were prepared by foundry route using high purity Al, Zn, Mg, and Al-2wt.%Sc master alloys. A small capacity muffle furnace was used to melting the aluminium alloys in laboratory scale (weight 4 kgs.). The rectangular size of cast plate ($200\times90\times24$ mm^3) was used to pour of liquid metal into a mild steel mould at a fixed 780°C for 2.5h in a graphite crucible while placed in the muffle furnace, then sequentially master alloy added into the melt with carefully control scandium fading effects. The chemical compositions of cast plates were analyzed by atomic absorption spectroscopy (AAS) and inductively coupled plasma atomic emission spectroscopy (ICP-AES) methods. The nominal compositions are listed below (in wt.%)-Zn+Mg = 10.30-13.91%, Zn: Mg >2, Sc varies 0.20-0.87 wt.% for a group of five aluminium alloys, and impurity contents of Si+Fe = 0.04-1.30% (max.), and balance of Al. The cast plate was preferred for suitable solution treatment (465°C for 1h) then immediately quenching in water (i.e., T_4). Subsequently, solution heat treated plate was selected for low temperatures artificial ageing treatment at 120°C, 140°C, and 180°C for 24h (T_6 alloy), as well as recorded Vicker's hardness (Model no.: FIE VM50 PC) measurements instantaneously for each slot with the average of six indentations with a typical standard deviation of ±5, and thoroughly plotted hardness bar diagrams in each of prepared alloy as shown in Figure 7(a). The ageing kineties also were characterized through sequentially Vicker's hardness measurements to evaluate the activation energies (Q, kJ/mole) at 120-180°C for 24h ageing time as shown in Table 1. The T_4 heat treated plates were preferred for FSP with variable parameters are 1000 rpm, 720 rpm, and 70 mm/min, 80 mm/min traverse speeds with constant 15 kN axial load, and specified tool design then subjected to post ageing treatment at 140°C for 2h (SFA). It has to mentioned that all FSP parameters and specified a tool design and sketching as shown in Table 2 and Figure 1(b), respectively. It is clear that post ageing treatment conducted after completion of double passes FSP plates, then the experimental samples were picked up carefully from SZ and preferred for several characterizations to revealing light optical microscopy to observe the nanosized precipitates in the matrix. The studied alloys had been thoroughly examined by OM, EPMA, FESEM, SEM for fractography analysis, and TEM analysis. The samples were collected from SZ and cut into small pieces then grounded, and polished with emery papers by sequentially 800, 1000, 1200, 1500, and 2000 grades, respectively. Then the cloth polishing was carried out with mechanically rotating wheel with adding of liquid Al_2O_3 particles until fine scratches have been removed. Then the sample was cleaned with water and dried using a hot air dryer and etched with modified Keller's reagent (20 ml HNO_3 (conc.), 3 ml HCl (conc.), 2 ml HF (48%), 175 ml distilled water). The optical microscope (Model no.: LEICA DMI 5000M, Leica Microsystems, Buffalo Grove, IL) used for the study was several microscopic analyses as shown in Figures 3 and 4. The cast sample was micro-segregation analyzed by EPMA (Model no.: CAMECA SX100) with EDS analysis as shown in Figure 2(a). The TEM samples were manually polished to obtain around 100 μm thinning down with scratches free and mirror finish surface. Then the samples were finally polished using twin-jet electro-polisher (solution content 75% CH_3OH and 25% HNO_3) at 12 V and -35°C (Model no.: Techai G^2 20 S-TWIN at 200 kV) as shown in Figures 5 and 6. The stress-strain curves had generated by using an Universal Testing Machine (Model no.: 25 kN, H25 K-S, UK) with a gradual cross head speed (1 mm/min) at room temperature, while tensile samples were picked up from SZ with properly machined from processed plate and results from computerized stress-strain curves are shown in Figure 7(b-d). The compact tension (CT) specimens

were picked up from SZ of FSP alloys. The FSP plates were preferred for notch preparation by CNC cutting machine (Sprintcut 734) along the SZ, while specimens to evaluated the fracture toughness properties as per ASTM E-399 standard. The CT was conducted as per optimized parameters such as 1000 rpm, 720 rpm, and 70 mm/min, 80 mm/min traverse speeds and measured variable heat input ratios (1000/70=14.3, 720/80 = 9) on the plate dimensions of 62.5×62×6.25 mm^3 after double passes FSP plates as shown in Figure 1(d). The fatigue pre-cracking was done in under the tension-tension mode using fatigue testing machine (Model no.: UTM Instron-8802) at frequency of 2 Hz, R of 0.1, and fatigue load of 800 N, respectively. The crack was created by applying fixed fatigue load as given in Table 3. The failed specimens were studied carefully for propagation of fracture path by SEM analysis (Model no.: LEO 435VP) as shown in Figure 1(c, d).

Table 1. *Results of activation energies (Q, kJ/mole) for three studied aluminium alloys.*

The activation energies (Q, kJ/mole) calculated based on the Arrhenius equation. (Sc varies 0.2-0.63 wt.% as increasing mode)						
Ageing time (h)						
0.5 h	**2 h**	**6 h**	**10 h**	**16 h**	**20 h**	**24 h**
9.56	9.96	14.57	11.76	15.37	16.89	20.38
6.34	7.51	14.10	13.40	16.31	22.56	30.45
5.72	7.62	5.72	28.01	16.24	18.34	22.33

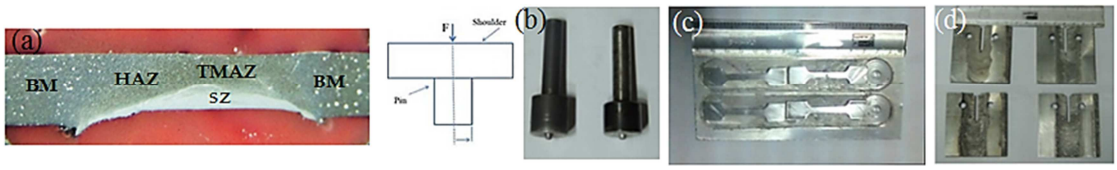

Figure 1. *(a) Macrograph of the double passes FSP sample, (b) The sketching a tool and related design, (c) Tensile specimens picked up from longitudinal direction in SZ after double passes FSP as per ASTM E8/E8M-11 standard, (d) The illustration of fracture toughness (K_{IC}) specimens as per ASTM E-399 standard.*

Table 2. *Processing parameters of FSP.*

FSP parameters and the tool design						
Tool rotation speed (rpm)	**Traverse speed (mm/min)**	**Friction pressure (up-setting force) (kN)**	**Pin angle (o)**	**Pin root diameter and height (mm)**	**No. of passes**	**Plate dimensions in mm^3**
1000	70	15	2.5	5.0 and 3.5	two	150×90×8

Table 3. *Processing parameters of fracture toughness (K_{IC}) test after FSP.*

FSP and fatigue parameters related K_{IC} test						
Tool rotation speeds (rpm)	**Traverse speeds (mm/min)**	**Friction pressure (up-setting force) (kN)**	**Tool design**	**Fatigue parameters and crack length on the notch tip**	**No. of passes**	**Plate dimensions in mm^3**
720, 1000	80, 70	15	Similar Table 2	Load=800 N, R (stress ratio) =0.1, 2 Hz, No. of cycles =1200, Crack length = 0.25 mm	two	62.5× 62 ×6.25

3. Results and Discussion

3.1. Evaluate Activation Energy and Related Fracture Toughness (K_{IC}) After FSP

The high strength aluminium alloys (7xxx series) are mainly popular for age-hardening ability in room temperature as well as elevated temperature due to decomposition of the supersaturated solid solution (SSSS), and the formation of GP zones, ή, and stable η and T precipitates [19-21]. The peak hardening effects and microstructural changes are depending on between GP-zones and nucleation of ή/η and nucleation of dislocations, and the diffusion of Zn to Mg atoms and GP-zones developed by artificial ageing treatments applied to cast aluminium alloys. The kinetics of the activation energy was evaluated for three different types of alloy system by the Vicker's hardness measurement during ageing treatments between 120-180°C. Due to scandium additions in high strength Al-Zn-Mg alloys have improved the mechanical properties by grain refinement in cast structure. It is noted that scandium did not form any compounds with Zn and Mg but its additive effect promising. Depending on the Zn to Mg ratios (>2) of the alloys effective precipitation sequences may be observed: SSSS→GP→ή→η ($MgZn_2$). Many researchers had been measured the activation energy for GP-I zone formation to be in the range of 0.59-0.67 eV or close to the migration energy for Mg in Al of 0.6 eV. The GP-II is not a dominant phase during T_6 ageing treatment (at the GP zones range) of these alloys. The ageing time and temperature are main two parameters to calculated for the experimental activation energies (Q, kJ/mole) at the temperature ranges 120-180°C by the Arrhenius equation as shown in Table 1. The graphical curve with ln(ΔHV) vs. 1/T gives a straight line with a slope of - Q/R, while the basic equation followed by $\Delta HV = HV_o \exp(-Q/RT)$, where ΔHV is the increased hardness at temperature T (K), HV_o is a constant term, Q of activation energy, and R of universal gas constant. The precipitation and dissolution of the precipitates transformation is always related to the perception of the lower activation energy can be attributed due to formation GP zones and nanosized Al_3Sc particles. It is noteworthy that the typically several binary

alloys such as Al-Zn, Al-Mg, Al-Si exhibited higher activation energies (>100 kJ/mole) rather than for ternary and scandium added quaternary aluminum alloy systems have lower activation energies due to nanosized Al_3Sc particles that the greater difficulty to migration of dislocations in the presence of hardening dispersoids for high stacking faults energy of aluminium alloys [22-25].

During FSP, agglomeration of the nanosized Al_3Sc particles were deliberately fragmented while increasing particles density in the matrix. The tensile strength improved first then decline gradually as well as fracture strength also reduces depending on variable scandium contents (eg. 0.20-0.87wt.%) and its effect as greater extend observe in the matrix as shown in Figure 7(b-d). The increase in tensile strength at room temperature is propose to be ascribed to the relatively even distribution of the nanosized Al_3Sc particles and ή precipitates, but at elevated temperature strengthening mechanism is quite different because only nanosized particles possess high thermal stability to boost the strength. It has to found that the tensile properties of these alloys are significantly influenced by the spatial distribution of the nanosized particles as shown in TEM analysis (Figures 5 and 6). The inhomogeneously distributed coarse particles can act as a crack source and preferential of crack propagation may lead to the fracture in the alloys. The EPMA micrograph with EDS spots analysis also hinted several irregular shapes and white Al_3Sc chunky particles scattered in the matrix. The higher scandium contents (usually hypoeutectic composition) are mostly thermodynamically favourable to formed such coarse particles and revealed high scandium concentrations in several spots as well as high Zn contents and Zn/Mg ratios (>2) are hinted spontaneous age-hardening ability in these alloys [26, 27]. The GB segregation and high impurity contents laterally varies from low to high concentrations for five prepared aluminium alloys are the most deleterious problems effectively impede the fracture strength, fracture toughness (K_{IC}) and diminish the scandium effects in the cast aluminium alloys. Notably, the fracture toughness in aluminium alloys is associated with an increasing strain hardening (i.e., n values of 0.19-0.21) [28], while scandium varies 0.2-0.45 wt.%. Many researchers agreed that the small size of inclusions facilitated in a significant enhancement in toughness is critically affected by the interparticle spacing between the inclusions and varies with inversely proportional to size of particles. Chen and Knott's hinted on the mechanical properties and the associated fracture behaviour of aluminium alloys, the relationship $K_{IC} \simeq 14.2362 \times n \times \sqrt{\sigma_y}$ describes the fracture toughness (K_{IC}) to the yield stress (σ_y, or $\sigma_{0.2\%}$), and also can be calculated with similarity of experimental value of K_{IC} =33.10 MPa$\sqrt{m}$ (refer from Figure 7c). The microstructural features apparent during the studied alloys can be influenced the fracture toughness such as the coarse intermetallics (typically Fe rich Mg_2Si, Al_3Sc chunky particles), the ageing precipitates and the grain structures. The fracture toughness (K_{IC}) of alloys containing the fine grains and nanosized particles enriched typically which are non-shearable and strongly bonded to the matrix. The FSP is widely used for controlling the microstructures of metallic materials for increasing the mechanical properties [29-38].

3.2. EPMA and FESEM Analysis of Studied Aluminium Alloys

The common characteristics of aluminium alloys are high volume fraction of alloying elements, which lead to severe dendrites and GB segregation in preferential sites. The EPMA observation indicated the high solute contents on GBs of cast alloys with EDS analysis (10 spots are recorded) as shown in Figure 2(a). Some of the spots analysis reveal high scandium (14.97wt.%) contents with high amount of impurities (Fe+Si) and major amount of oxides are exhibited in matrix. It is observed that the high amount of Zn and Mg retained in a solid solution is mostly similar concentration as investigated during AAS and ICP-AES analyses. A large quantity of rod like or plate like and network eutectic primary particles $T(Mg_{32}(Al, Zn)_{49})$ are dispersed in the interdendritic regions and on GBs as shown in TEM analysis in Figures 5 and 6. Since the percentage of area accounted by GBs are much higher in the alloy containing scandium, their partitioning effect must be increased with scandium additions. On the other hand, Al_3Sc particles did not suppress the formation of ageing precipitates in aluminium alloys, although a fine dispersion of coherent nanosized Al_3Sc particles enhanced strengthening of the alloys. Some researchers had reported that the nanosized Al_3Sc particles perfectly corresponding to the $L1_2$ structure when they form during homogenization treatment. The nucleation of precipitates on dislocation begins with the interaction between the solute atom and the dislocation phenomenon. As well, the interaction of vacancies and lattice impurities with dislocation leads to distortion in the surrounding crystal. At 140°C ageing process has revealed highest hardening effect due to formation of GP-II zones plus nanosized Al_3Sc particles and transform to ή phases in the matrix [39]. It has been showed optimum hardening effect of hardness at 380-390HV in 2-6h ageing time and its achieved due to high density of nanosized particles and ή-phases united effects as well as beneficial effects have nearly equal size of lattice parameters within the solvent solid solution can be easily nucleated in the matrix. Figure 2(b, c) shows FESEM micrographs with EDS analysis of cast and T_4 aluminium alloys, and EDS spot analysis have been identified lower concentrations of Zn and Mg, and high amount of impurities (Fe+Si= 0.45-1.28 wt.%) as well as scandium contents (4.61-17.25wt.%) in the matrix. It is noted that cast alloys clearly exhibited enormous amount of segregation on the GBs but its deleterious effects completely eliminated after T_4 heat treatment as well as scandium effectuality rise multiple times than actual alloy contents. In contrary, at T_6 heat treatment clearly exhibited GB segregation with high amount of impurities (Fe+Si=13.31 wt.%) existing but scandium concentrations laterally decline (17.25-7.77 wt.%) in the matrix as shown Figure 2(d).

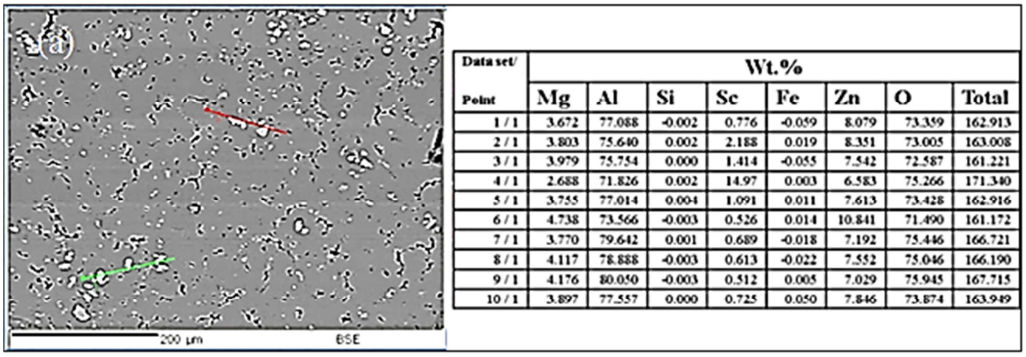

Data set/ Point	Wt.%							
	Mg	Al	Si	Sc	Fe	Zn	O	Total
1 / 1	3.672	77.088	-0.002	0.776	-0.059	8.079	73.359	162.913
2 / 1	3.803	75.640	0.002	2.188	0.019	8.351	73.005	163.008
3 / 1	3.979	75.754	0.000	1.414	-0.055	7.542	72.587	161.221
4 / 1	2.688	71.826	0.002	14.97	0.003	6.583	75.266	171.340
5 / 1	3.755	77.014	0.004	1.091	0.011	7.613	73.428	162.916
6 / 1	4.738	73.566	-0.003	0.526	0.014	10.841	71.490	161.172
7 / 1	3.770	79.642	0.001	0.689	-0.018	7.192	75.446	166.721
8 / 1	4.117	78.888	-0.003	0.613	-0.022	7.552	75.046	166.190
9 / 1	4.176	80.050	-0.003	0.512	0.005	7.029	75.945	167.715
10 / 1	3.897	77.557	0.000	0.725	0.050	7.846	73.874	163.949

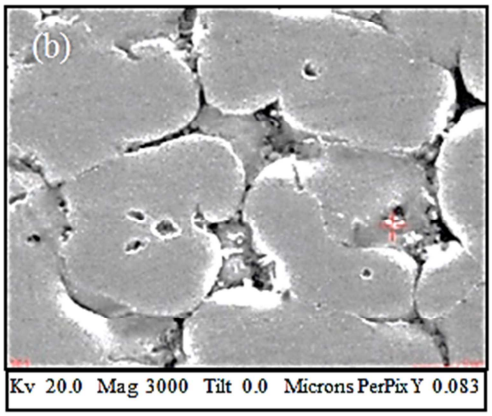

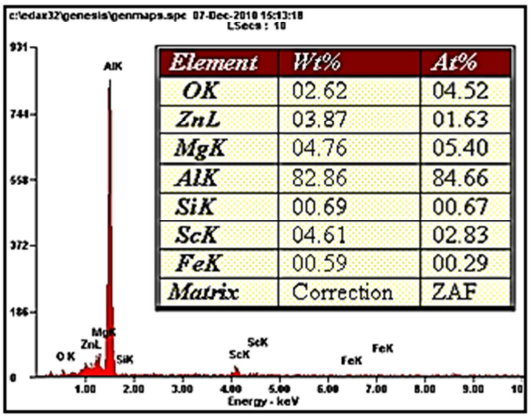

Element	Wt%	At%
OK	02.62	04.52
ZnL	03.87	01.63
MgK	04.76	05.40
AlK	82.86	84.66
SiK	00.69	00.67
ScK	04.61	02.83
FeK	00.59	00.29
Matrix	Correction	ZAF

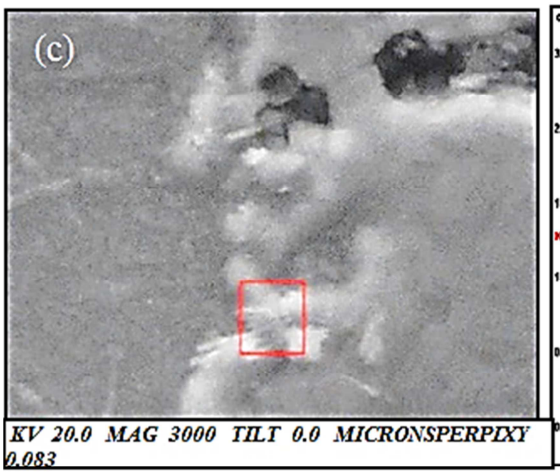

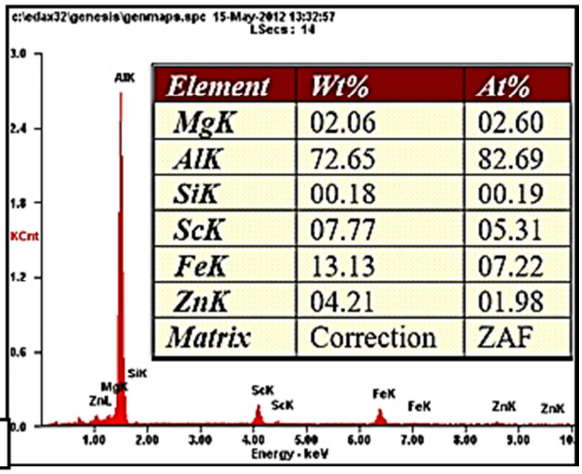

Element	Wt%	At%
MgK	02.06	02.60
AlK	72.65	82.69
SiK	00.18	00.19
ScK	07.77	05.31
FeK	13.13	07.22
ZnK	04.21	01.98
Matrix	Correction	ZAF

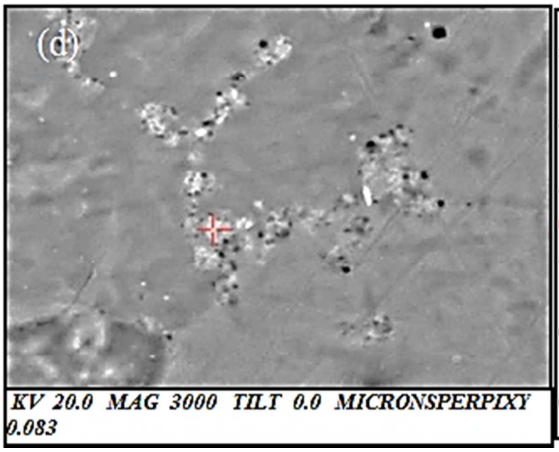

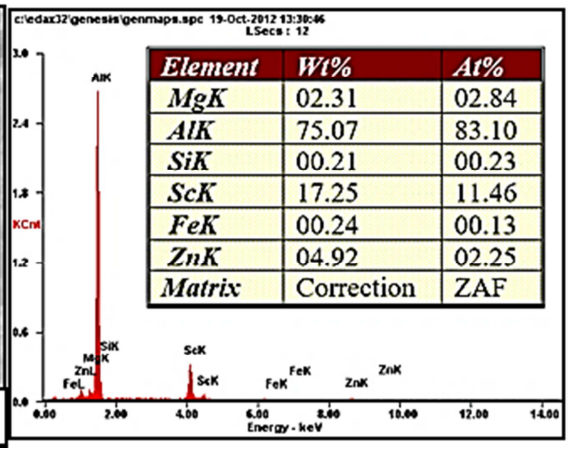

Element	Wt%	At%
MgK	02.31	02.84
AlK	75.07	83.10
SiK	00.21	00.23
ScK	17.25	11.46
FeK	00.24	00.13
ZnK	04.92	02.25
Matrix	Correction	ZAF

Figure 2. *EPMA and FESEM micrographs with EDS analysis at three different conditions: (a, b) As-cast condition, (c) T_4, and (d) T_6 analysis in studied aluminium alloys (Sc varies 0.2-0.45 wt.% as increasing mode).*

3.3. Microstructural Analysis of T_6 and FSP Conditions

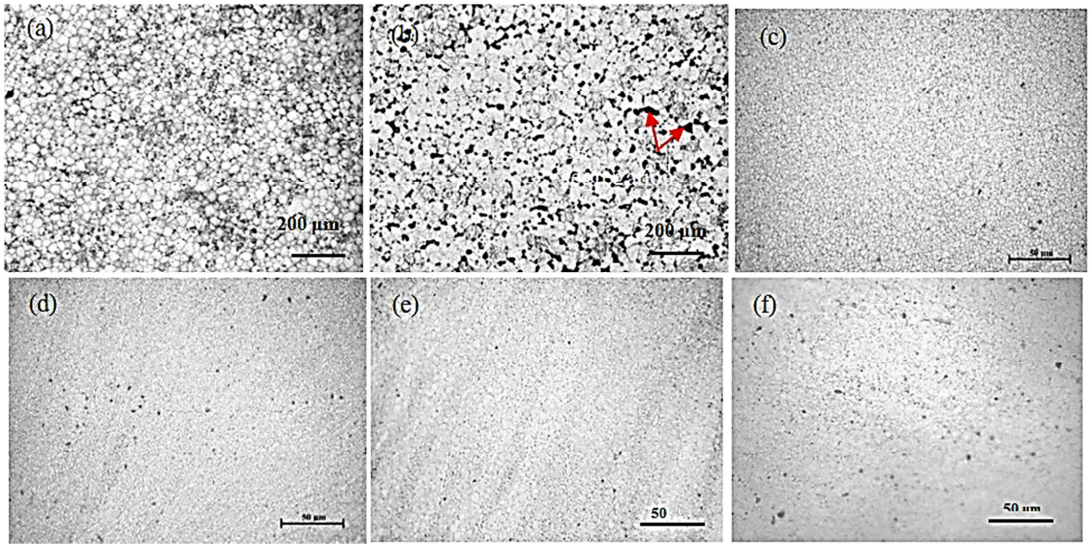

Figure 3. *Optical micrographs of studied aluminium alloys: (a, b) Aged at 140°C for 6h (T_6), and aged at 120°C for 20h (T_6); (c, d) after FSP, and (e, f) SFA condition (Sc varies 0.2-0.45 wt.% as increasing mode).*

The microstructures exhibited laterally fine equiaxed grains and fine precipitates and eliminated GB segregations after T_6 heat treatments as shown in Figure 3 (a, b). There are significant grain refinements obtained by promoting heterogeneous nucleation sites during solidification, suggesting that the primary Al_3Sc particle serve as an effective grain nucleant, while the amount of scandium exceeds the eutectic contents that the accelerated ageing kinetics, and anti-recrystallization for nanosized Al_3Sc particles finely dispersed to enhance thermal stability and improved the mechanical properties after T_6 conditions. It is generally accepted that underaged microstructure consists of GP zones and it may or may not be coexist with peak aged ή phases with nanosized Al_3Sc particles [40]. The high mechanical properties of cast aluminium alloys have mainly associated with the fine grain strengthening caused by the addition of variable scandium contents and chemical hardening and precipitation strengthening of nanosized particles and η precipitates during T_6 ageing treatments. If T_6 ageing time is increasing at 120°C for 20h, their massive microstructural changes likely grain coarsening as well as GB over burning due to coarse constituents are showing several black spots throughout the matrix as shown in Figure 3(b). Notably, the increase in ageing precipitates can diminish fracture resistance, because these precipitates are the major contributors to the strength of alloys. Figure 3(c-f) shows the SZ microstructures with uniformly distributed fine grains due to DRX mechanism which led to frictional force between the FSP tool pin and working plate induced heat resulting recrystallized processed zone. It can be seen that SZ microstructures constitutes finely distributed grains with less numbers of precipitates. It might be that during the stirring action, the most hardening phases were dissolved, but at the same time nanosized Al_3Sc particles helped in retaining the fine grains surrounding by high angle grain boundaries which was free from dislocations. As well, revealing the SZ microstructures with equiaxed grains along with the formation of inner subgrains surrounding by high angle grain boundaries. In these cases, the formation of inner subgrains was assisted by the nanosized Al_3Sc particles suppressed the recrystallization mechanism by hindering the dislocation motion and Zener pinning on the GBs. In view of OM observations, it can be concluded that the vicinity of GBs create minute hair line cracks with several black spots are observed, it was due to plasticized action which led to the intense heat generation to resulting Zn vaporization occurs after SFA. At the minor scandium contents, grains typically refined, equiaxed and achieved about 1-2 µm then gradually grains are become coarser as higher scandium contents (eg. hypereutectic composition) as well as Al_3Sc chunky particles fragmented and scattered due to vigorous stirring action of FSP throughout the matrix, resulting fine precipitates but grains laterally become marginally coarser approximately above 2-6 µm. Figure 4(a-c) shows the SEM micrographs after as-cast and FSP at variable scandium contents, but it has to noted that Al_3Sc chunky particles strongly exist typically on the GBs or scatters smaller sizes in the cast aluminium alloys. The EDS analysis shows that rich in scandium chunky particles of 36.70 wt.% and 35.37 wt.% in cast and FSP conditions, respectively. On the other hand, the scandium activity reduces along with high impurity contents (Fe+Si = 13.61 wt.%) are increasing and other element like zinc (3.09 wt.%) loss as a result of numerous black holes formed due to Zn vaporization (red arrows) effects observe in the matrix as shown in Figure 4(c). Apart from this, nanosized Al_3Sc particles and microstructural changes like DRX induced by FSP and Orowan strengthening and the movement of dislocations due to presence of nanosized particles are liable for fine grains and enhancement of hardness in SZ. Specially, nanosized Al_3Sc particles and age hardening precipitates confine the movement of grains which in turn diminishes the

grain growth and causes DRX [41, 42].

3.4. Characterization of Scandium Agglomeration Tendency Through SEM Analysis

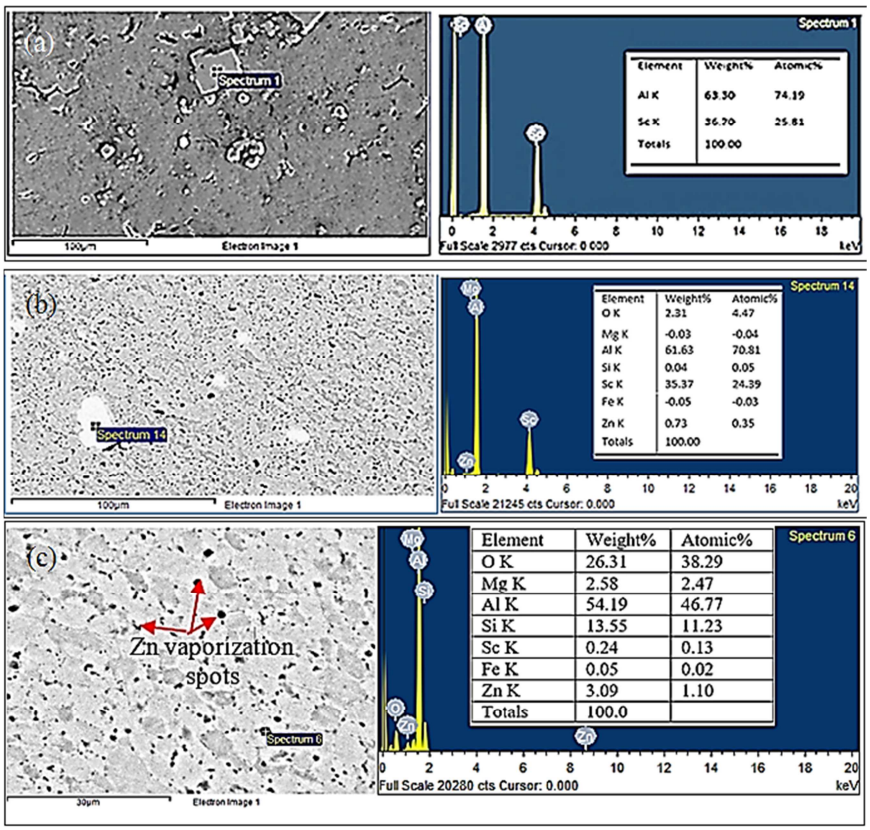

Figure 4. *(a) SEM micrograph with EDS analysis of cast aluminium alloy, (b, c) SEM micrographs with EDS analysis after FSP (Sc varies 0.2-0.87 wt.% as increasing mode).*

3.5. TEM Observation With EDS Analysis of T_6 Aluminium Alloys

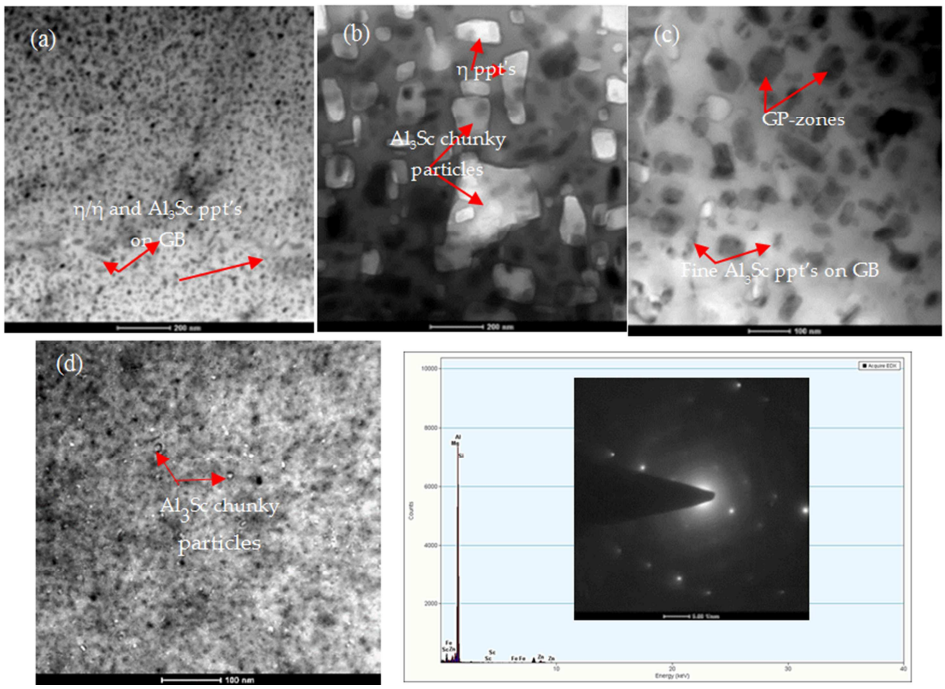

Figure 5. *(a-d) Illustration of TEM micrographs with EDX and SAD patterns of studied aluminium alloys (Sc varies 0.2-0.87 wt.% as increasing mode) at T_6 condition (low and high magnifications).*

Figure 5 (a-d) shows the TEM micrographs with EDS analysis of T_6 aluminium alloys (140°C for 6h). The highly dense ή (metastable) hardening precipitates and nanosized Al_3Sc dispersoids identified by EDS with SAD analysis. The nanosized particles distribution of 5-15 nm is dominated in the matrix, and the nanosized Al_3Sc particles increased with increasing scandium concentrations in these alloys as shown in Figure 5(a). Figure 5 (b, c) shows the TEM micrographs with SAD pattern of cast aluminium alloys after T_6 condition at different magnifications. There are two dominated nanosized particles are identified such as a cauliflower shape of Al_3Sc particles (~30-50 nm) usually pinning down on the GBs and clearly visible in different magnifications in the matrix. In contrast, a needle shape ή/η particles (red arrows) are notably visible in specified magnification (~20-50 nm) seems these particles have interacted with dislocation tangles or inserted on GBs also effectively impede the movement of dislocations, and a high density of dislocations is also detected in the matrix. It is noteworthy that a good interfacial bonding without cracks or apparent interfacial reaction between the nanosized Al_3Sc particles and α-Al matrix, it possesses high thermal stability and promoting considerably the tensile strength at elevated temperature can be observed. Therefore, it is mentioned that nanosized Al_3Sc particles diminish the grain size of aged aluminium alloys that the generating Hall-Patch or grain refinement strengthening obtained by the equation: $\sigma_{H-P} = \sigma_o + kd^{-0.5}$ where k of 0.04 MPa√m, and increased yield strength as $\Delta\sigma_{H-P}$ could be calculated individually about 6 MPa. Apart from this, a lot of hardening precipitates fragmented and several black holes (red arrows) are visible most probably Zn vaporization defects exerted owing to high heat input energy (1.1-1.4 kJ/mm) during FSP as shown in Figure 5(d) [43, 44]. The defects will eventually become crack initiation points and leading to fracture failure of these alloys.

3.6. TEM Observation with Variable Scandium Contents After SFA

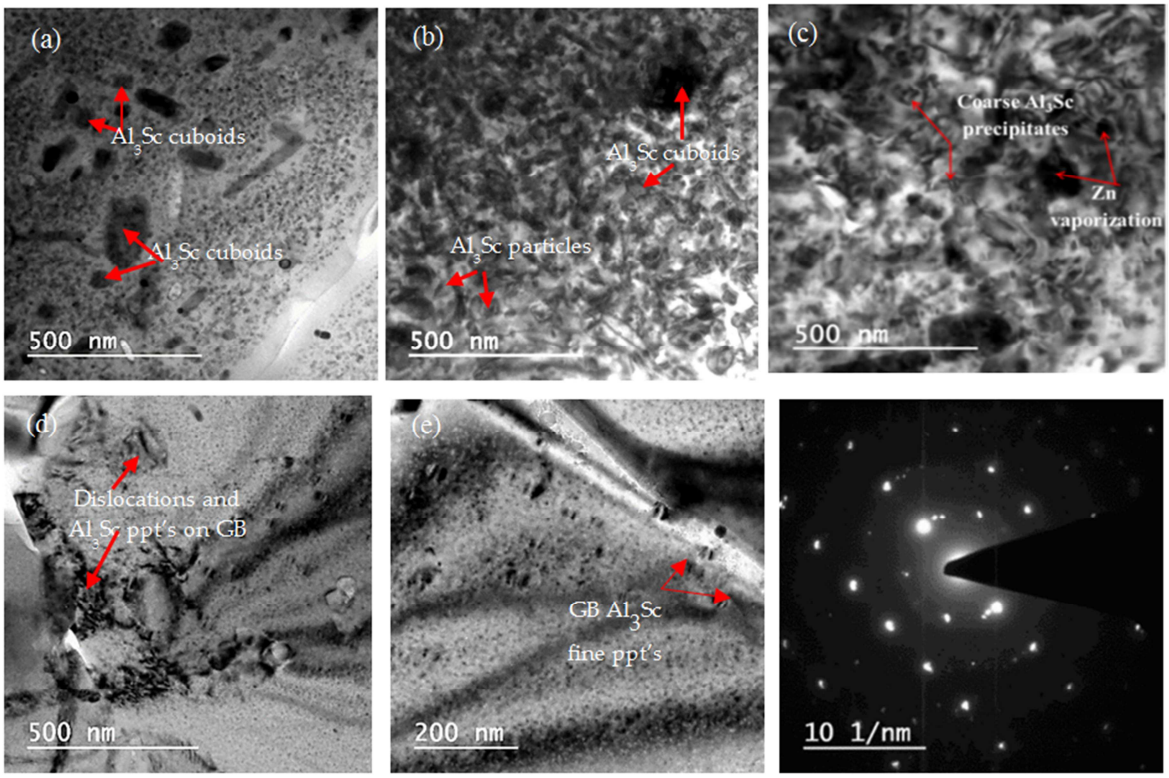

Figure 6. *(a-e) Illustration of TEM micrographs with SAD pattern of studied aluminium alloys (Sc varies 0.2-0.87 wt.% as increasing mode) at SFA condition (low and high magnifications).*

Figure 6(a-e) shows TEM micrographs with SAD pattern mainly exhibited fine distribution of ή, Al_3Sc particles in matrix. It is noted that as increasing scandium contents their precipitates morphology are changing drastically towards the higher scandium contents in the matrix. It is clearly specified several coarse constituents scatter randomly that the enhanced alloy chemistry depend on higher scandium contents as well as uniform distribution of fine submicroscopic precipitates plus large precipitates become cuboid with Al_3Sc particles in the matrix. The TEM micrographs have revealed finely distribution with different shape and size of precipitates due to nanosized Al_3Sc particles may be accelerated after SFA condition. These particles are firmly interaction with the GBs and dislocations may tends to toughen the SZ region during deformation with thermal treatment. TEM micrographs with SAD analysis have shown high density of fine precipitates disperse randomly throughout in matrix, but there are few bright spots

perhaps for Al_3Sc cuboids (indicated by red arrows) around the centre of diffraction pattern in the matrix. At higher magnification (200 nm), its clearly indicated effective Zener pinning effects on the GB by cauliflower shape of Al_3Sc nanosized particles (~30-50 nm) in the matrix. Thus, TEM micrographs of aluminium alloys exhibited fine precipitates of ή phases (usually needle shape and size ~ 5-20 nm) and existence of Al_3Sc particles with some black holes formed due to Zn vaporization defects in matrix. Meanwhile, the strong pinning force from nanosized particles on the grain/subgrain boundaries can impede the migration during thermal deformation, leading to restricted grain growth of SFA aluminium alloys. Instead, nanosized Al_3Sc particles can avert the dislocation motion as a result of boost precipitation strengthening, and due to larger effective particle sizes (>100 nm) the precipitation strengthening occurs through the Orowan bypass mechanism rather than shear mechanism hinted in TEM analysis, also Orowan strengthening or grain/subgrain boundary strengthening can be focused in the matrix [45].

3.7. Age-Hardening Effects, Fracture Strength and Toughness at Variable Scandium Contents

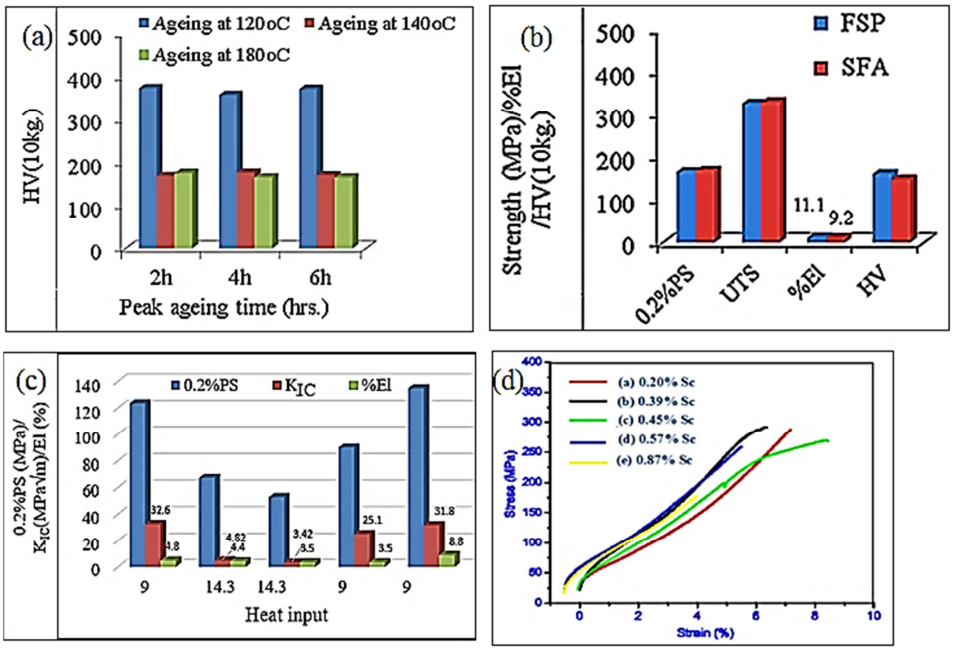

Figure 7. *(a) Showing Vicker's hardness bar diagrams as selected peak hardness at different ageing temperatures, (b) Illustration of mechanical properties of studied alloys at two different conditions after FSP and SFA, (c) Fracture toughness (K_{IC}) profiles vs. Heat input ratios (rpm/traverse speed) after FSP, (d) The conventional stress-strain curves as Sc varies 0.2-0.87 wt.% with variable Zn/Mg ratios of studied aluminium alloys after SFA.*

Figure 7(a) shows the age hardening effects on the hardness at 120°C for different studied alloys. The peak aged stability regime was obtained after few hours within 2-6h of 24h ageing interval. The peak aged stability regime has been extended due to the addition of scandiums, and also exhibited peak hardness values of 380-390 HV. The peak aged stability regime has extended as well as reveal higher hardening response that is the main function of nanosized Al_3Sc particles with GP-zones activity mainly prominent, and ή hardening phases intensely highlighted in SEM and TEM analyses. It is clearly observed that the peak aged formation due to high scandium contents (eg. hypereutectic composition), which controlled to the formation of Al_3Sc particles, and these particles encouraged anti-recrystallization action as the solute contents increase, which further increase the hardness due to more Zener pinning effect formed during the interaction with the dislocations and GBs. The ageing strengthening results from impeding the dislocations motion by the precipitates, and the interaction between dislocation and precipitate occurs by two different prominent mechanisms such as non-shear and shear mechanisms. The non-shear (Orowan) mechanism is leading for the ageing strengthening of these alloys, when the size of the precipitate is below the critical size. It has expected that scandium additions providing the additional site for the nucleation of precipitates in aluminium matrix. It is mostly adding of higher scandium contents in the alloys deliberately enhanced the peak hardness. Figure 7(b) shows bar diagrams of tensile properties revealed after FSP and SFA conditions of studied aluminium alloys. The high strength has achieved due to uniform distribution of hardening precipitates (ή/η) with nanosized Al_3Sc particles dispersoid in matrix, it has also revealed in TEM micrographs (Figures 5 and 6). After SFA condition, the strength of the alloys marginally increased but ductility decline about 1.9%, ultimate tensile strength (UTS) of 329 MPa, 0.2% proof strength (0.2%PS) of 169 MPa, and hardness in SZ about 147.8HV, respectively [46]. The main strengthening mechanisms are grain refinement, dispersion hardening as well as dissolution of hardening phases due to intense plastic deformation during FSP creates optimal heat input energy (1.1-1.4 kJ/mm). The heat input energy is also responsible for DRX mechanism of grain refinement that the ascribed balance mechanical

properties such as optimum hardness accomplished in SZ about 150-170HV after FSP. Figure 7(c) shows that several bar diagrams have been exhibited 0.2% PS about 120-135 MPa, ductility about 4.5-9.0%, and fracture toughness (K_{IC}) about 4.82-32.6 MPa√m at variable scandium contents with Zn/Mg ratios, impurity contents, and most importantly heat input ratios (i.e., rpm/traverse speed), respectively. In the present work, the lower heat input ratio of 9 is exhibited effective role to withstand better fracture toughness of 25-32.6 MPa√m indicates fine distribution of nanosized Al_3Sc particles (~30-50 nm) in TEM analysis at lower concentration of scandiums (eg. hypoeutectic composition), but at high heat input ratio of 14.3 have lower fracture toughness of 3.5-4.4 MPa√m [47]. Although SZ have recrystallized finer grains, 0.2% PS and hardness are lower as variable scandium contents (eg. hypereutectic composition). This may be due to dissolution of finer precipitates and agglomeration tendency of Al_3Sc chunky particles during FSP which needs further examination [48, 49]. On the other hand, PFZ beside the GB usually play an important role on the fracture toughness (K_{IC}), wide PFZ will create additional strain localization, which may inspire GB failure resulting in facilitating the intergranular failure and weakening the fracture resistance [50]. Thus, the nanosized particles and the fracture toughness (K_{IC}) of the alloy is correlated to the Young's modulus (E), yield strength ($\sigma_{0.2\%}$), and λ can be estimated by the following equation: $K_{IC} = 2\sigma_{0.2\%}$ Eλ, but λ is an inter-particle spacing with function of size (d), and volume fraction (V) of these particles: $\lambda = d(\pi/6V)^{1/3}$, i.e., in constant V of nanosized particles, the Orowan strength is better when the particles are smaller in size [51]. The conventional stress-strain curves with variable scandium contents and Zn/Mg ratios have the major influences on the fracture strength and ductility after SFA condition. The mechanical properties such UTS, 0.2% PS, fracture strength and elongation were evaluated and presented in the Figure 7(d). It has observed that UTS, fracture strength and ductility improved with increases of gradual scandium contents (eg. hypoeutectic composition) their combined effects due to grain refinement and presence of nanosized Al_3Sc particles with high input energy and high input ratios (rpm/traverse speed) which causes more softening tendency in the SZ because of stirring action of the tool pin. This perhaps due to strengthening mechanisms such as Orowan strengthening and dislocation density detected in TEM analysis as shown in Figure 6(b-d). It also observed the elongation and fracture strength (i.e., ~4% and 178 MPa) both are decreases drastically due to presence of Al_3Sc chunky particles as gradually increases with scandium up to 0.87 wt.% which may lead to increase of slip distance of dislocations during deformation of SFA alloys. In addition, the higher fracture strength and ductility values are achieved at variable scandium contents (eg. hypoeutectic composition) such as about 288-270.5 MPa and 6.8-5.6% in consecutively depend on the variable scandium contents (eg. 0.39, 0.45, and 0.57 wt.%), but optimum tensile properties are achieved such as fracture strength and ductility likely 273 MPa and 6.8% at 0.39wt.% Sc content among the all studied aluminium alloys [52]. The SEM(T) fractography was characterized by SEM with EDS analysis to understand the failure patterns and revealed agglomeration of Al_3Sc chunky particles as hypereutectic scandium contents (>0.6 wt.%) in the matrix.

3.8. Observation of SEM (T, CT) Fractography Images

The failed tensile fracture surfaces are examined by SEM analysis after SFA as showing mostly fine dimple-type intergranular fractures in the matrix as shown in Figure 8(a-f). The intergranular fractures propagation mechanism is markedly visible with no existence of Al_3Sc chunky particles in matrix. The cracks are intensely following through the GBs due to preferential coarse precipitates or Al_3Sc chunky particles in case of higher scandium contents and agglomeration type of syndrome as shown in Figure 8(e, f). If PFZ adjacent to the high angle grain boundaries and indirectly affect the intergranular ductile fractures, and coupled with the presence of coarse and closely spaced GB precipitates initiate the fractures. While nanosized Al_3Sc particles can effectively restrict the formation of PFZ in these alloys. There is currently available a reasonable amount of experimental information after SEM with EDS analysis revealed accumulation of Al_3Sc chunky particles after SFA. Since it is the metallurgical process stirring action in the SZ which governor the deformation and fracture behaviour of a cracked specimens, it is appealing to attempt to correlation the resultant toughness with other mechanical properties in these alloys. The nature of metal flow in the SZ, large clusters of Al_3Sc particles or Zn vaporization defects (Figure 4c and Figure 5d) are formed that the preferential path of fracture during tensile deformation. Based on these results, it is evident that the nanosized Al_3Sc/Al matrix display a combination of optimal tensile properties and fracture toughness and without loss of ductility. Although the nanosized particles activity attend to alter the composition, density and microstructure, such as the change in the ή/η precipitates size depend on Zn to Mg ratios that the major reasons for the enhancement can be ascribed to the reduction of volume fraction of casting defects and their size of the micropores after tensile deformation. Specially, the larger and more plentiful pre-existing micropores in the aluminium alloys would serve to intensify the process of microvoids coalescence and thereby accelerate the cracking resulting in a reduce stress required for final fracture and a lesser fracture toughness [53, 54]. In addition, fairly narrower widths of PFZs lead to a higher fracture toughness for nanosized Al_3Sc particles containing alloys usually exhibit more discontinuous precipitation on GB that the useful to improving GB fracture resistance and fracture toughness (K_{IC}) of studied aluminium alloys. In the case of SEM (CT) fracture surfaces exhibited entirely intergranular mode with continuous cracks propagation path concentrate surrounding Al_3Sc chunky particles or Zn vaporization defects, and coarse intermetallic particles (Fe-rich and Mg_2Si) fracture and decohesion comprise very minute plastic energy dissipation cracks, and a fracture dominated by coarse particle cracks in

the alloys leading to low toughness as shown in Figure 8(g, h) [55-58].

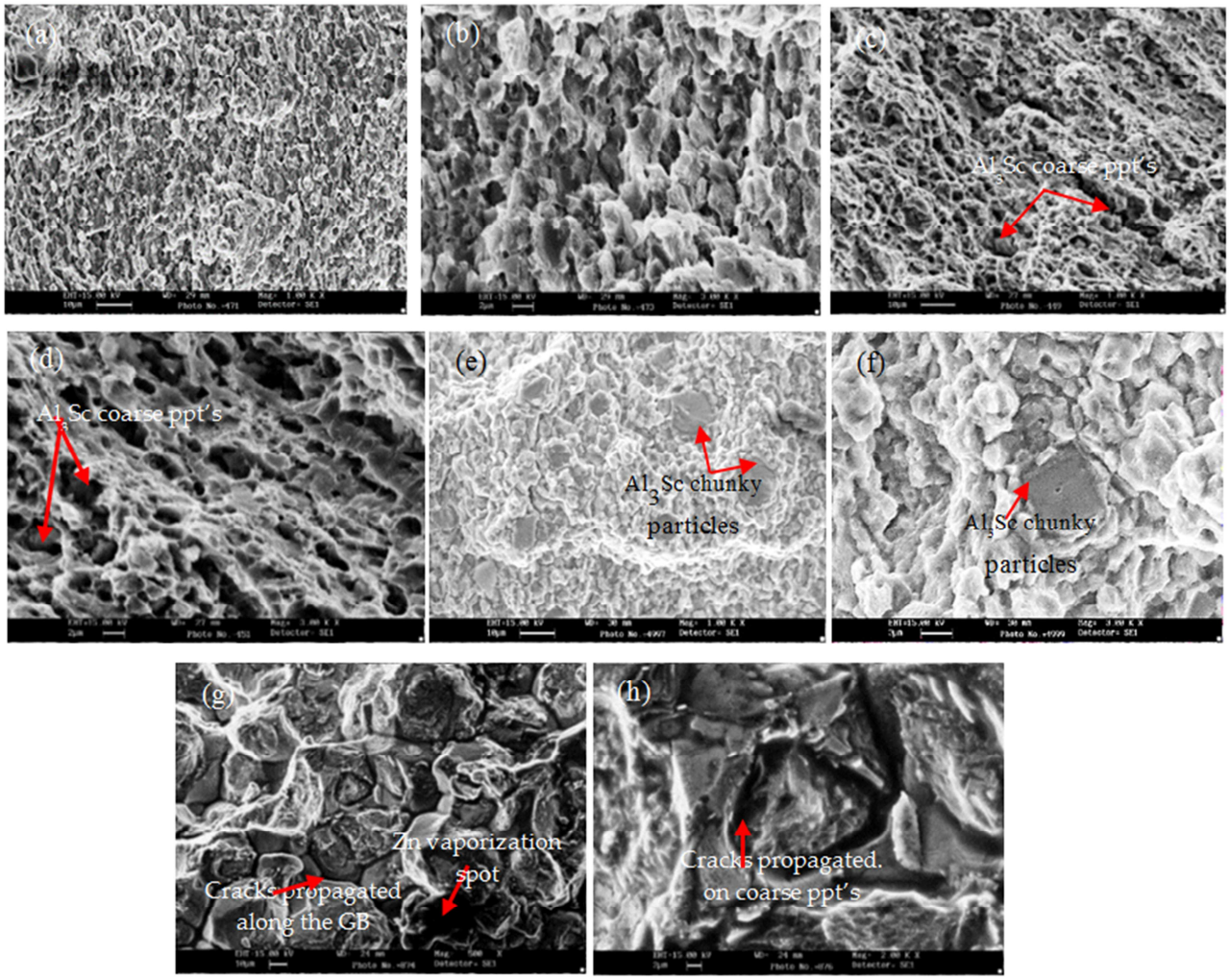

Figure 8. *(a-f) SEM (T) fractography images after SFA, and (g, h) SEM (CT) fractography images after FSP (Sc varies 0.45-0.87 wt.% as increasing mode) (low and high magnifications).*

4. Conclusions

1. Due to scandium additions in high strength Al-Zn-Mg alloys (7xxx series) have improved the mechanical properties by grain refinement in cast structure. It is noted that scandium did not form any compounds with Zn and Mg but its additive effect promising.
2. The precipitates transformation mechanism is always related to the perception of the lower activation energy (max. Q, 30.45 kJ/mole at 24h) can be attributed due to formation of GP zones and nanosized Al_3Sc particles.
3. In view of optical microscopy (OM) observations, it can be concluded that the vicinity of GBs create minute hair line cracks with several black spots are observed, it was due to plasticized action which led to the powerful heat generation to resulting Zn vaporization defect occurs after SFA.
4. The nanosized particles are identified such as a cauliflower shape of Al_3Sc particles (~30-50 nm) usually pinning down on the GBs and clearly visible in different magnifications in TEM analysis of T_6 alloys. In contrast, a needle shape ή/η particles (red arrows) (~20-50 nm) are notably visible in specified magnification seems these particles have interacted with dislocation tangles or inserted on GBs also effectively impede the movement of dislocations, and a high density of dislocations is also detected in the matrix.
5. The high strength has accomplished due to uniform distribution of hardening precipitates (ή/η) with nanosized Al_3Sc particles dispersoid in the matrix. The main strengthening effects are boosted due to precipitation strengthening and dispersion strengthening of nanosized particles and hardening phases, but after SFA the alloys strength marginally increased such as UTS of 329 MPa, 0.2%PS of 169 MPa, and hardness in SZ about 147.8HV as well as ductility slightly decline about 1.9%, respectively.
6. At higher magnification (200 nm), its clearly indicated

effective Zener pinning action on the GBs by cauliflower shape of nanosized Al_3Sc particles (~30-50 nm) in the matrix. Thus, TEM micrographs of these aluminium alloys exhibited fine precipitates of ή/η phases (usually needle shape and size ~5-20 nm) with some black holes formed due to Zn vaporization defects in matrix.

7. The SEM (CT) fracture images exhibited entirely intergranular mode with few ductile dimples imply with continuous cracks propagation path primarily concentrate surrounding Al_3Sc chunky particles or Zn vaporization defects, and coarse intermetallic particles (Fe-rich and Mg_2Si) fracture and decohesion comprise very little plastic energy dissipation cracks, and a fracture dominated by coarse particle cracks in these alloys leading to low fracture toughness (eg. 3.42 MPa√m).
8. The plain strain fracture toughness (K_{IC}) values of studied aluminium alloys have been achieved likely 25.1-32.6 MPa√m at variable scandium contents (eg. hypoeutectic composition) and two typical FSP parameters are efficiently focused on likely optimum heat input energy (1.1-1.4 kJ/mm) and low heat input ratio (i.e., 9), respectively.
9. The present fracture strength and ductility are achieved at variable scandium contents (eg. hypoeutectic composition) such as about 288-270.5 MPa and 6.8-5.6% in consecutively depend on the variable scandium contents (eg. 0.39, 0.45, and 0.57 wt.%), but optimum tensile properties are achieved such as fracture strength and ductility likely to 288 MPa and 6.8% at 0.39wt.% Sc contents among the all studied aluminium alloys.

Acknowledgments

The author was financially supported during Ph. D works for MHRD fellowship by the Department of Metallurgical and Materials Engineering, Indian Institute of Technology Roorkee (IITR), Uttarakhand State-247667, India.

References

[1] Emani S. V., Benedyk J., Nash P., Chen D. (2009). Double ageing and thermomechanical heat treatment of AA7075 aluminium alloy extrusions. Jr. of Mat. Sci., 44, 6384-6391.

[2] Kim J. H., Yeom J. T., Hong J. K., Shim S. Y., Lim S. G. Park N. K. (2010). Effect of Scandium on the Hot extrudability of 7075 Aluminium Alloy. Metals and Mat. Inter., 16, 4, 669-677.

[3] Costa S., Puga H., Barbosa J., Pinto A. M. P. (2012). The effect of Sc addition on the microstructure and age hardening behaviour of as cast Al-Sc alloys. Mat. and Design, 42, 347-352.

[4] Ferragut R., Somoza A., Tolley A., Torriani I. (2003). Precipitation kinetics in Al-Zn-Mg commercial alloys. Jr. of Mat. Proc. Tech., 41, 35-40.

[5] Ahmed Z. (Feb. 2003). The properties and Application of Scandium-Reinforced Aluminium, Jr. of the Minerals, Metals and Mat. Society (JOM), 55, 2, 35-39.

[6] Royset J., Ryum N. (2005). Scandium in aluminium alloys. Inter. Mat. Reviews, 50, 1, 19-44.

[7] Deng Y., Yin Z, Zhao K., Duan J., He Z. (2012). Effects of Sc and Zr microalloying additions on the microstructure and mechanical properties of new Al-Zn-Mg alloys. Jr. of Alloys and Comp., 530, 71-80.

[8] Loffler H., Kovacs I., Lendvai J. (1983). Review Decomposition processes in Al-Zn-Mg alloys. Jr. of Mat. Sci., 18, 2215-2240.

[9] Wu L-M., Wang W-H., Hsu Y-F., Trong S. (2008). Effects of homogenization treatment on recrystallization behaviour and dispersoid distribution in an Al-Zn-Mg Sc-Zr alloy. Jr. of Alloys and Comp., 456, 163-169.

[10] Ma Z. Y. (March 2008). Friction Stir Processing Technology: A Review. Met. and Mat. Trans. A, 39A, 642-658.

[11] Cavaliere P., Squillace A. (2005). High temperature deformation of friction stir processed 7075 aluminium alloy. Mat. Characterization, 55, 136-142.

[12] Rhodes C. G., Mahoney M. W., Bingel W. H., Calabrese M. (2003). Fine-grain evolution in friction-stir processed 7050 aluminium. Scripta Mat., 48, 1451-1455.

[13] Liu J., Guo F., Wang T., Duan S., Zou Y. (2023). Study on corrosion resistance of HAZ and TMAZ in friction stir welding joint of 7075 aluminium alloy by thermal simulation. Mater. Res. Express, 10, 1-13.

[14] Deng Y., Ye R., Xu G., Yang J., Pan Q., Peng B., Cao X., Duan Y., Wang Y., Lu L., Yin Z. (2015). Corrosion behaviour and mechanism of new aerospace AL-Zn-Mg alloy friction stir welded joints and the effects of secondary $Al_3Sc_xZr_{1-x}$ nanoparticles. Corrosion Sci., 90, 359-374.

[15] Liu J., Guo F., Wang T., Duan S., Zou Y. (2023). Study on corrosion resistance of HAZ and TMAZ in friction stir welding joint of 7075 aluminium alloy by thermal simulation. Mater. Res. Express, 10, 1-12.

[16] Nascinmento, F., Santos T., Vilaca, P., Miranda, R. M., Quintino L. (2009). Microstructural modifications and ductility enhancement of surfaces modified by FSP in aluminium alloys. Mat. Sci. and Eng. A, 506, 16-22.

[17] Kurt A., Uygur I., Cete E. (2011). Surface modification of aluminium by friction stir processing. Jr. of Mat. Processing Tech., 313-317.

[18] Ku M-H., Hung F-Y., Lui T-S., Chen L-H., Chiang W-T. (2012). Microstructural Effects of Zn/Mg Ratio and Post Heat Treatment on Tensile Properties of Friction Stirred Process (FSP) Al-xZn-yMg Alloys. Mat. Trans., 53, 5, 995-1001.

[19] Chen J., Zhen L., Yang L., Shao W., Dai D. (2009). Investigation of precipitation behaviour and related hardening in AA 7055 aluminium alloy. Mat. Sci. and Eng. A, 500, 34-42.

[20] Afify N., Gaber A-F., Abbady G. (2011). Fine Scale Precipitates in Al-Zn-Mg Alloys after Various Aging Temperatures, Mat. Sc. and Appl., 2, 427-434.

[21] Engdahl T., Hansen V., Warren P. J, Stiller K. (2002). Investigation of fine scale precipitates in Al-Zn-Mg alloys after various heat treatments. Mat. Sci. and Eng. A, 327, 59-64.

[22] Sha W. (2006). Activation energy for precipitation hardening and softening in aluminium alloys calculated using hardness and resistivity data. Physica Status Solidi (a), 203, 8, 1927-1933.

[23] Juhasz A., Kovacs I., Lendvai J., Tasnadi P. (1985). Initial clustering after quenching in AlZnMg alloys. Jr. of Mat. Sci., 20, 624-629.

[24] Nandam S. H., Sankaran S., Murty B. S. (Feb.-April 2011). Precipitation kinetics in Al-Si-Mg/TiB_2 in-situ composites. Trans. of The Indian Ins. of Metals, 64, 1-2, 123-126.

[25] Abo Zeid E. F., Gaber A. (Dec. 2012). MECHANICAL PROPERTIES AND PRECIPITATION BEHAVIOUR AS A FUNCTION OF HEAT TREATMENT OF Al-4.4Cu-1.5Mg-0.6Mn-0.25Si (WT.%) ALLOY. Int. Jr. of Met. & Mat. Sc. and Tech. (IJMMSE), 2, 4, 11-20.

[26] Mukhopadhyay A. K. (April 2009). Microstructure and properties of high strength aluminium alloys for structural applications. Trans. of the Indian Ins. of Metals, 62, 2, 113-122.

[27] Yu J., Li X. (2011). Modelling of the Precipitated Phases and Properties of Al-Zn-Mg-Cu Alloys. Jr. of Phase Equilibria and Diff., 32, 4, 350-360.

[28] Chemingui M., Khitouni M., Mesmacque G., Kolsi A. W. (2009). Effect of heat treatment on plasticity of Al–Zn–Mg alloy: Microstructure evolution and mechanical properties. Physics Procedia, 2, 1167-1174.

[29] Gaber A., Gaffar M. A., Mostafa M. S., Abo Zeid EF. (2007). Precipitation kinetics of Al-1.12Mg2Si-0.35Si and Al-1.07Mg2Si-0.33Cu alloys. Jr. of Alloys and Comp., 429, 167-175.

[30] Mandal P. K. (2016). Study on GP-Zones Formation in the Sc Inoculated Ternary Al-Zn-Mg Alloys. Jr. of Met. & Mat. Eng. (JoMME), 6, 2, 53-69.

[31] Thompson D. S. (1975). Metallurgical factors affecting high strength aluminium alloy production. Metall. Trans. A, 6A, 671–683.

[32] Reddy A. C., Rajan S. S. (2005). Influence of ageing, inclusions and voids on ductile fracture mechanism in commercial Al-alloys. Bull. Mater. Sci., 28, 75–79.

[33] Wagner J. A., Shenoy R. N. (1991). The effect of copper, chromium, and zirconium on the microstructure and mechanical properties of AlZn-Mg-Cu alloys. Metall. Trans. A., 22A, 2809–2818.

[34] Kamp N., Sinclair I., Starink M. J. (2002). Toughness-strength relations in the overaged 7449 Al-based alloy. Metall. and Mater. Trans. A., 33A, 1125–1136.

[35] Chen K., Liu H., Zhang H., Li S., Todd R. I. (2003). The improvement of constituent dissolution and mechanical properties of 7055 aluminium alloy by stepped heat treatments. Jr. Mat. Process. Tech., 142, 190–196.

[36] Han N. M., Zhang X. M., Liu S. D., He D. G., Zhang R. (2011). Effect of solution treatment on the strength and fracture toughness of aluminium alloy 7050. Jr. Alloy. and Comp., 509, 4138–414.

[37] Hornbogen E., Starke E. A. (1993) Theory assisted design of high strength low alloy aluminium. Acta Metall. Mater., 41, 1–16.

[38] Furuhara T., Maki T. (2001). Variant selection in heterogeneous nucleation on defects in diffusional phase transformation and precipitation. Mater. Sci. Eng. A, 312, 145–154.

[39] Liu C. Y., Zhang B., Ma Z. Y., Teng G. B., Wei L. L., Zhou W. B., Zhang X. Y. (2018). Effects of pre-ageing and minor Sc addition on the microstructure and mechanical properties of friction stir processed 7055 Al alloy. Vacuum, 149, 106-113.

[40] Zhenbo H., Zhimin Y., Sen L., Ying D., Baochuan S., Xiang Z. (August 2010). Preparation, microstructure and properties of Al-Zn-Mg-Sc alloy tubes. Jr. of Rare Earths, 28, 4, 641-646.

[41] Dakarapu S. R., Nallu R. (2017). Process parameters optimization for producing AA6061/TiB2 composites by friction stir processing. Jr. of Mech. Eng., 67, 1, 101-118.

[42] Ihara K., Miura Y. (2004). Dynamic recrystallization in Al-Mg-Sc alloys. Materials Sci. and Eng. A, 387-389, 647-650.

[43] Kumar A., Gautam S. S., Kumar A. (2014). HEAT INPUT & JOINT EFFICIENCY OF THREE WELDING PROCESSES TIG, MIG AND FSW USING AA6061. Int. Jr. Mech. Eng. & Rob. Res., 1, 1, 89-94.

[44] Ju X.; Zhang F., Chen Z.; Ji G., Wang M., Wu Y., Zhong S., Wang H. (2017). Microstructure of Multi-Pass Friction-Stir-Processed Al-Zn-Mg-Cu Alloys Reinforced by Nano-Sized TiB_2 Particles and the Effect of T_6 Heat Treatment. Metals, 7, 530, 1-15.

[45] Deng Y., Yang Z., Zhang G. (2020). Nanostructure Characteristics of $Al_3S_{1-x}Zr_x$ Nanoparticles and Their Effects on Mechanical Property and SCC Behavior of Al-Zn-Mg Alloys. Materials, 13, 1909, 1-11.

[46] Mandal P. K. (2021). Effect of Sc on solidification segregation and subsequent friction stir processing of aluminium alloy. Mat. Todays: Proc., 44, 1050-1057.

[47] Pradeep S., Pancholi V. (2013). Effect of microstructural inhomogeneity on superplastic behaviour of multipass friction stir processed aluminium alloy. Mat. Sci. & Eng. A, 561, 78-87.

[48] Siveraj P., Kanagarajan D., Balasubramanian V. (June 2014). EFFECT OF POST WELD HEAT TREATMENT ON FRACTURE TOUGHNESS PROPERTIES OF FRICTION STIR WELDED AA7075-T651 ALUMINIUM ALLOY JOINTS. Jr. of Manuf. Eng., 9, 2, 110-115.

[49] Chen Z., Mo Y., Nie Z. (August 2013). Effect of Zn Content on the Microstructure and Properties of Super-high Strength Al-Zn-Mg-Cu Alloys. Meta. And Mat. Trans. A, 44A, 3910-3920.

[50] Yan A., Chen L., Liu H. S., Xiao E. F., Li X. Q. (2015). STUDY ON STRENGTH AND FRACTURE TOUGHNESS OF Al-Zn-Mg-Cu-Ti (-Sn) ALLOYS. Jr. of Mining and Met., Section B: Met., 51, 1, 73-79.

[51] Roshan M. R., Mirzaei M., Jahromi S. A. J. (2013). Microstructural characteristics and tensile properties of nano-composite Al 2014/4 wt.% Al_2O_3 produced from machining chips. Jr. of Alloys and Comp., 569, 111-117.

[52] Mandal P. K. (June 2017). Investigation of Microstructure And Mechanical Properties of Al-Zn-Mg and Al-Zn-Mg Alloys After Double Passes Friction Stir Processing. Int. Jr. of Mat. Sci. and Eng., 5, 2, 47-59.

[53] Yang C., Zhao Q., Zhang Z., Li L., Tian W., Liu R., Zhang P., Xu Y., Li Y., Zhang Z., Jiang Q., Ritchie R. O. (2020). Nanoparticle additions promote outstanding fracture toughness and fatigue strength in a cast Al-Cu alloy. Mat. and Design, 186, 1-8.

[54] Kumar P. V., Reddy G. M., Rao K. S. (2015). Microstructure, mechanical and corrosion behavior of high strength AA7075 aluminium alloy friction stir welds-effect of post weld heat treatment, Defence Tech., 11, 362-369.

[55] Ludka G. M., Laughlin D. E. (March 1982). The Influence of Microstructure and Strength on the Fracture Mode and Toughness of 7XXX Series Aluminium Alloys. Metall. Trans. A, 13A, 411-425.

[56] Dai Y., Yan L., Hao J. (2022). Review on Micro-Alloying and Preparation Method of 7xxx Series Aluminium Alloys: Progresses and Prospects. Materials, 15, 1216, 1-26.

[57] Morgeneyer T. F., Starink M. J., Sinclair I. (2006). Experimental analysis of toughness in 6156 Al-alloy sheet for aerospace applications. Mat. Sci. Forum, 519-521, 1023-1028.

[58] Garrett G. G., Knott J. F. (Sept. 1978). The Influence of Compositional and Microstructural Variations on the Mechanism of Static Fracture in Aluminium Alloys. Metall. Trans. A, 9A, 1187-1201.